CHAPTER

22

Synthesis of Folds in 3D with Bézier Surface

*Manash Pratim Gogoi**, *Soumyajit Mukherjee*†

*Department of Geology, Sibsagar College, Sivasagar, India †Department of Earth Sciences, Indian Institute of Technology Bombay, Powai, Mumbai, India

OUTLINE

BACKGROUND INFORMATION

Zulauf et al. (2017) stated that, "*As our observations are frequently linked by rock exposure, the geometric data obtained from natural folds are largely incomplete and often restricted to two dimensions.*" Folds (Hall, 1815), on the other hand, are three-dimensional curved structures produced in rocks in nature (usually) by ductile deformation. In 3D, the zone with maximum curvature is recognized as the hinge (Turner and Weiss, 1963), which becomes a point when visualized in only two dimensions. This hinge zone separates two usually differently oriented limbs (Fossen, 2016) that could either be curved or straight (Billings, 1954). Elements like hinge line, amplitude, wavelength, dip isogon, and interlimb angle have been defined to describe the fold conveniently in 2D profiles (e.g., Wegmann, 1929; Clark and McIntyre, 1951; Ramsay, 1967; Hudleston, 1973). On the other hand, the axial surface (Donath, 1964) is described in 3D in relation to the fold axis and the hinge line.

Folds have been studied in 3D based on hinge curvature or bluntness (Fossen, 2016), orientation of the hinge line and the hinge surface (Fleuty, 1964), cylindricity (Turner and Weiss, 1963), and superposition patterns of cylindrical folds (Ramsay, 1967). On the other hand, a class of noncylindrical sheath folds also exists that develop in high-strain shear zones (Cobbold and Quinquis, 1980; Alsop and Carreras, 2007; Wex et al., 2014; Mukherjee et al., 2015).

1 INTRODUCTION

Knowing 3D geometries of folds can lead to better decisions in exploration (e.g., Rowan, 1997). For that reason, geoscientists have been studying better classification of folds (Grose et al., 2017). Folds in 3D are rarely preserved in natural exposures available along almost three perpendicular directions (e.g., Alsop and Carreras, 2009). Fold geometries in 3D are more commonly encountered in structural geological literature when those folds are fault-related (e.g., Wilkerson et al., 1991). By linking a series of cross-sections deduced from field studies, one can have a 3D

https://doi.org/10.1016/B978-0-12-814048-2.00023-5
© 2019 Elsevier Inc. All rights reserved.

perspective of geological structures such as folds (Wilkerson et al., 1991, and references therein). Tipper (1976) discussed serial sectioning to explore 3D morphologies of structures, but its convincing application on folds seems lacking. Analytical modeling by Fletcher (1991), devoid of any software, studied folds in 3D. Lisle (1992) classified 3D fold morphologies into two types: (i) developing and (ii) nondeveloping. Ramón et al. (2013) X-rayed folded model materials and quantified their 3D morphologies. Yamamoto et al. (2014) picked up data from real geological objects and built up their morphological models. Cornish and Searle (2017) quantified 3D morphologies of natural folds based on high-resolution photographs. Zulauf et al. (2017) analytically modeled domes and basins in 3D. Analog modeling can simulate folds in a lab, but setting a dynamically scaled model is time consuming (e.g., folds developed in horizontal flow channel in Mukherjee et al., 2012). Free software are available online to extrapolate fold geometries by using some branches of structural geology such as cross-section balancing. Mathematical models can assist better visualization of surfaces in 3D.

Along with the advancement in scientific instrumentation and computation facility, efforts have been continuously made in 3D representation, visualization, modeling, and measurements of geological structures and exposures. Some of them include LiDAR (Light Detection And Ranging), photogrammetry and GPS mapping, Portable Extensible Toolkit for Scientific Computation (PETSc), and Lithosphere and Mantle Evolution Model (LaMEM). LaMEM develop finite-element-based landscape evolution models. Numerical models can involve differential geometry (Mynatt et al., 2007) with the aid of contiguous points with Gaussian curvature and mean curvature of consistent sign (Lisle and Toimil, 2007). 3D representation is also performed with seismic data (Rowan, 1997), virtual technology in image-based 3D modeling (Tavani et al., 2016), continuum mechanics, and finite element method (von Tscharner et al., 2016), which may involve software like Google Earth (de Paor et al. 2016), GOCAD (Wex et al., 2014), etc.

2 MODEL

Certain fold-related parameters viz., cylindricity, basal aspect, that is, the ratio of depth (D) to width (W), can further be experimented with the help of cubic Bézier surface as it provides 16 individual controlling points to alter the shape of a 2D (X-Y) plane in 3D (Z-Axis). The Bézier curve/surface and its operation in a computer give excellent flexibility to simulate a large variation in fold geometry. Therefore the Bézier equation would be important for students to learn. The Bézier surface is a mathematical polynomial interpolation possessing a set of control points. It was first described by Pierre Bézier in 1962 for its implicit use in designing automobiles.

The Bézier curves are two-dimensional geometric shapes that may be constructed in a Cartesian coordinate system into various forms (Gogoi et al., 2017). The fundamental equation of Bézier curve of degree m is (Vince, 2010; Janke, 2015; Sederberg, 2016):

$$C^m(u) = \sum_{i=0}^{m} P_i B_i^m(u) \qquad u \in [0, 1] \tag{1}$$

where P_i: location of controlling/handling points.

m: degree of curve. A set of $(m+1)$ numbers of control points P_0, P_1,…,P_m exist.

$B_{i,m}$: blending functions.

$B_{i,m}(u)$: Bernstein polynomials given by (Agoston, 2005; Vince, 2010):

$$B_{i,m}(u) = \binom{m}{i}(1-u)^{m-i}u^i, \quad i = 0, 1, \ldots, m \tag{2}$$

Here,

$$\binom{m}{i} : \text{binomial coefficient, i.e., } \frac{m!}{i!(m-i)!}$$

By understanding the shape of a cubic Bézier curve, it will be easy to alter the shape of the cubic Bézier surface. Fig. S1 in the online version at https://doi.org/10.1016/B978-0-12-814048-2.00023-5 presents a cubic Bézier curve with four controlling points viz. P_0, P_1, P_2 and P_3 with possible coordinates (0,0), (0,10), (10,10), and (10,0), respectively. Here, points P_0 and P_3 act as the starting and ending points, respectively, of the curve P_1 and P_2.

As per Fig. S1 in the online version at https://doi.org/10.1016/B978-0-12-814048-2.00023-5, a cubic Bézier curve with controlling points P_0, P_1, P_2, and P_3 could be drawn on the X–Z plane (Fig. S2 in the online version at

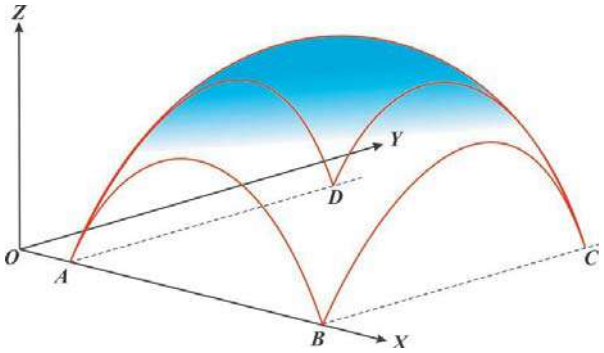

FIG. 1 An example of Bézier surface enveloping the Bézier curves AB, BC, CD, and AD.

https://doi.org/10.1016/B978-0-12-814048-2.00023-5) and can be repeated multiple times along the Y-direction. Now, a surface can be imagined enclosing these curves (in blue), which will mimic/represent these curves. Similarly, we can consider Bézier curves AB and DC on the XZ plane (Fig. 1), separated by distance BC or AD; and two more curves BC and AD on the YZ plane separated by distance AB or DC. The surface shown in Fig. 1 has been constructed from the interpolation of equations of these Bézier curves. This surface is the Bézier surface.

We can consider another Bézier curve of degree n such that each point P_i of the curve defined by Eq. (1) traverse the Bézier curve of degree n, then

$$P_i = P_i(v) = \sum_{j=0}^{n} P_{i,j} B_j^n(v) \qquad u \in [0,1] \tag{3}$$

Combining Eqs. (1) and (3), one obtains the point

$$C^{m,n}(u,v) = \sum_{j=0}^{n} \left[\sum_{i=0}^{m} P_{i,j} B_i^m(u) \right] B_j^n(v)$$

where

$$u, v \in [0,1] \tag{4}$$

Eq. (4) is the general equation of the Bézier Surface (Farin, 1997). To derive a quadratic Bézier surface, consider $m=n=2$, and the cubic Bézier surface will be of the order of $m=n=3$. Putting $m=3$ in Eq. (2):

$$B_{0,3}(u) = \binom{3}{0}(1-u)^{3-0}u^0 = (1-u)^3 \tag{5}$$

$$B_{1,3}(u) = \binom{3}{1}(1-u)^{3-1}u^1 = 3u(1-u)^2 \tag{6}$$

$$B_{2,3}(u) = \binom{3}{2}(1-u)^{3-2}u^2 = 3u^2(1-u) \tag{7}$$

$$B_{3,3}(u) = \binom{3}{3}(1-u)^{3-3}u^2 = u^3 \tag{8}$$

(the value of $\binom{3}{1}$ or $\binom{3}{2}$ is 3 as per Eq. 2 as they are factorial functions.

e.g. $\binom{3}{2} = \frac{3!}{2! \times (3-2)!} = \frac{3 \times 2 \times 1}{2 \times 1} = 3$

Similarly,

$$B_{0,3}(v) = \binom{3}{0}(1-v)^{3-0}v^0 = (1-v)^3 \tag{9}$$

$$B_{1,3}(v) = \binom{3}{1}(1-v)^{3-1}v^1 = 3v(1-v)^2 \tag{10}$$

$$B_{2,3}(v) = \binom{3}{2}(1-v)^{3-2}v^2 = 3v^2(1-v) \tag{11}$$

$$B_{3,3}(v) = \binom{3}{3}(1-v)^{3-3}v^2 = v^3 \tag{12}$$

Now Eq. (4) of order $m = n = 3$, will have 16 numbers of controlling points ($P_{i,j}$). Substituting Eqs. (5) to (12) into Eq. (4):

$$\begin{aligned} C^{3,3}(u,v) = &\left[P_{0,0}(1-u)^3 + P_{1,0}3u(1-u)^2 + P_{2,0}3u^2(1-u) + P_{3,0}u^3\right](1-v)^3 \\ &+ \left[P_{0,1}(1-u)^3 + P_{1,1}3u(1-u)^2 + P_{2,1}3u^2(1-u) + P_{3,1}u^3\right]3v(1-v)^2 \\ &+ \left[P_{0,2}(1-u)^3 + P_{1,2}3u(1-u)^2 + P_{2,2}3u^2(1-u) + P_{3,2}u^3\right]3v^2(1-v) \\ &+ \left[P_{0,3}(1-u)^3 + P_{1,3}3u(1-u)^2 + P_{2,3}3u^2(1-u) + P_{3,3}u^3\right]v^3 \end{aligned} \tag{13}$$

Eq. (13) is an extended form of Eq. (4) of degree 3. It provides 16 controlling points ($P_{i,j}$). Each controlling point has three values in 3D coordinate reference system (x, y, z) and by providing these values, the shape of the surface could be constrained.

As in Table 1, a surface (Fig. 2) constructs in Wolfram Mathematica program using the following source code in notebook (*.nb format):

TABLE 1 Coordinates of Controlling Points of the Cubic Bézier Surface

Controlling point	Coordinate (x, y, z)	Example	Controlling point	Coordinate (x, y, z)	Example
$P_{0,0}$	$x_{0,0}, y_{0,0}, z_{0,0}$	0, 0, 0	$P_{2,0}$	$x_{2,0}, y_{2,0}, z_{2,0}$	2, 0, 0
$P_{0,1}$	$x_{0,1}, y_{0,1}, z_{0,1}$	0, 1, 0	$P_{2,1}$	$x_{2,1}, y_{2,1}, z_{2,1}$	2, 1, 0
$P_{0,2}$	$x_{0,2}, y_{0,2}, z_{0,2}$	0, 2, 0	$P_{2,2}$	$x_{2,2}, y_{2,2}, z_{2,2}$	2, 2, 0
$P_{0,3}$	$x_{0,3}, y_{0,3}, z_{0,3}$	0, 3, 0	$P_{2,3}$	$x_{2,3}, y_{2,3}, z_{2,3}$	2, 3, 0
$P_{1,0}$	$x_{1,0}, y_{1,0}, z_{1,0}$	1, 0, 0	$P_{3,0}$	$x_{3,0}, y_{3,0}, z_{3,0}$	3, 0, 0
$P_{1,1}$	$x_{1,1}, y_{1,1}, z_{1,1}$	1, 1, 0	$P_{3,1}$	$x_{3,1}, y_{3,1}, z_{3,1}$	3, 1, 0
$P_{1,2}$	$x_{1,2}, y_{1,2}, z_{1,2}$	1, 2, 0	$P_{3,2}$	$x_{3,2}, y_{3,2}, z_{3,2}$	3, 2, 0
$P_{1,3}$	$x_{1,3}, y_{1,3}, z_{1,3}$	1, 3, 0	$P_{3,3}$	$x_{3,3}, y_{3,3}, z_{3,3}$	3, 3, 0

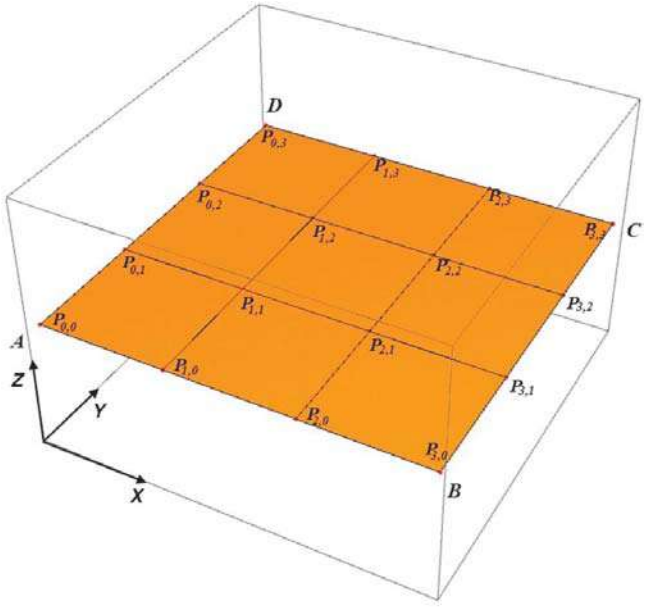

FIG. 2 3D plot of the cubic Bézier surface plotted with coordinates listed in Table 1. The difference between the surface shown in Fig. 3 and this surface is that there have been "zero" Z-values assigned to all controlling points of this surface.

```
pts = {{{0, 0, 0}, {0, 1, 0}, {0, 2, 0}, {0, 3, 0}}, {{1, 0, 0}, {1, 1, 0}, {1, 2, 0},
      {1, 3, 0}}, {{2, 0, 0}, {2, 1, 0}, {2, 2, 0}, {2, 3, 0}}, {{3, 0, 0}, {3, 1, 0},
      {3, 2, 0}, {3, 3, 0}}};
f = BézierFunction[ pts]
BézierFunction[{{0., 1.}, {0., 1.}}, <>]
Show[Graphics3D[{PointSize[Medium], Red, Map[Point, pts]}], Graphics3D[{Black,
Line[pts], Line[Transpose[pts]]}], ParametricPlot3D[f[u, v], {u, 0, 1}, {v, 0, 1},
Mesh -> None]]
```

Now, the surface (Fig. 2) that will appear on execution of the above source code will be flat 2D plane *ABCD* (plotted in 3D reference system), as all of the controlling points have *z*-values = 0.

Now, only by changing the *z*-values by 1 for the four central controlling points viz. $P_{1,1}$ (1,1,1), $P_{1,2}$ (1,2,1), $P_{2,1}$ (2,1,1), and $P_{2,2}$ (2,2,1), the surface *ABCD* (Fig. 2), can be converted into a curved surface (Fig. S3 in the online version at https://doi.org/10.1016/B978-0-12-814048-2.00023-5). The following coordinates were added in the notebook for execution:

```
pts = {{{0, 0, 0}, {0, 1, 0}, {0, 2, 0}, {0, 3, 0}},{{1, 0, 0}, {1, 1, 1}, {1, 2, 1},
      {1, 3, 0}},{{2, 0, 0}, {2, 1, 1}, {2, 2, 1}, {2, 3, 0}},{{3, 0, 0}, {3, 1, 0},
      {3, 2, 0}, {3, 3, 0}}};
```

PROBLEM 1: SIMULATE A SYNCLASTIC ANTIFORM. A SYNCLASTIC SURFACE IS A CURVED SURFACE WITH PRINCIPLE RADII OF CURVATURE IN TWO PERPENDICULAR DIRECTIONS EXCEED ZERO (LEMAITRE, 2009).

Solution: The surface *ABCD* shown in Fig. S3 in the online version at https://doi.org/10.1016/B978-0-12-814048-2.00023-5 takes an anticlinal domal shape. However, altering the values of coordinates of other points will change the shape of the surface differently. Similarly, a cylindrical fold can be derived from the same surface, the curve *AB* and *CD* should be identically folded (by putting similar *z*-value to two mid-controlling points), and keeping *AD* and *BC* equal and parallel (Fig. 3A). Subsequently, if we modify curve *AD* and *BC* also, then this cylindrical fold converts to a synclastic antiform (Fig. 3B). Note the mathematical term "synclastic" connotes that the centers of the two principal curvatures occur at the same side of the surface. In an opposite case, they are called "anticlastic" (Lisle and Toimil, 2007). Such a fold geometry was also described in mathematical models by Lisle and Toimil (2007). To change the shape of the surface *ABCD* into a cylindrical fold and synclastic antiform: (a) For a cynlindrical fold (Fig. 3A):

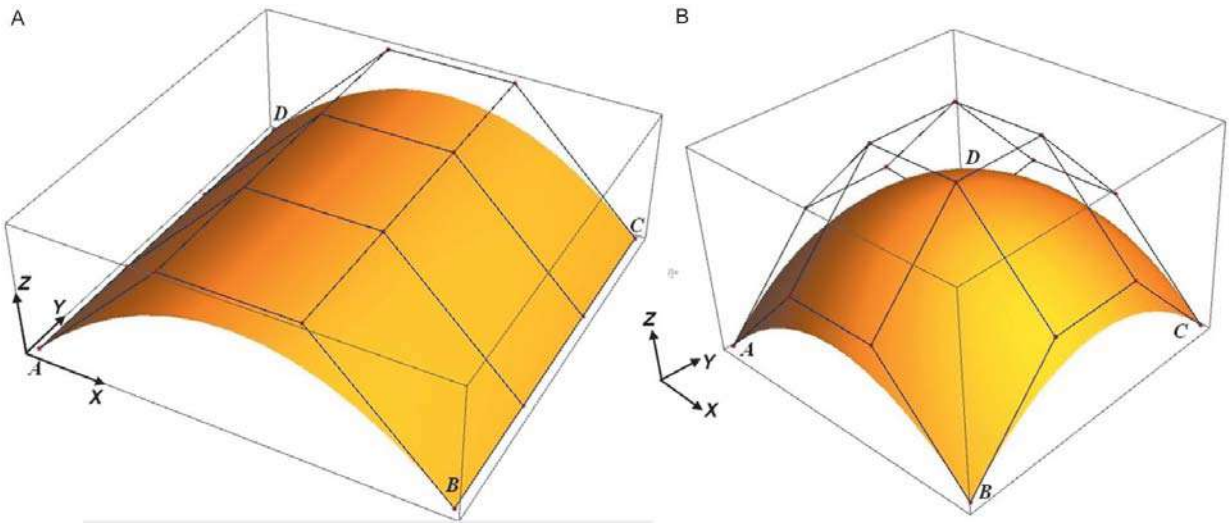

FIG. 3 3D view of a (A) cylindrical fold and (B) synclastic antiform constructed from Bézier surface.

```
pts = {{{0, 0, 0}, {0, 1, 0}, {0, 2, 0}, {0, 3, 0}},
      {{1, 0, 1}, {1, 1, 1}, {1, 2, 1}, {1, 3, 1}},
      {{2, 0, 1}, {2, 1, 1}, {2, 2, 1}, {2, 3, 1}},
      {{3, 0, 0}, {3, 1, 0}, {3, 2, 0}, {3, 3, 0}}};
```

(b) for a synclastic antiformal fold (Fig. 3B):

```
pts = {{{0, 0, 0}, {0, 1, 1}, {0, 2, 1}, {0, 3, 0}},
      {{1, 0, 1}, {1, 1, 2}, {1, 2, 2}, {1, 3, 1}},
      {{2, 0, 1}, {2, 1, 2}, {2, 2, 2}, {2, 3, 1}},
      {{3, 0, 0}, {3, 1, 1}, {3, 2, 1}, {3, 3, 0}}};
```

Either (*AB – CD)* or (*AD – BC*) curves could be modified to construct a cylindrical fold (Fig. 3A). Now by observing the relation between the curves and controlling points of the surface *ABCD* (Fig. S3 in the online version at https://doi.org/10.1016/B978-0-12-814048-2.00023-5), different types of folds can be plotted in 3D by changing the coordinates of the controlling points.

For instance, Fig. 4A shows an upright cylindrical symmetric fold. This fold can be further modified by shifting intermediate controlling points viz. $P_{1,0}$, $P_{2,0}$, $P_{1,1}$, $P_{2,1}$, $P_{1,2}$, $P_{2,2}$, $P_{1,3}$, and $P_{2,3}$ synchronously along the *X*-axis laterally, into asymmetrical folds (Fig. 4B–F). Construction of recumbent folds (Fig. 4G), requires to change the ending controlling points $P_{0,0}$, $P_{0,1}$, $P_{0,2}$, and $P_{0,3}$ by adding elevation and, similar *x*-values but different *z*-values for intermediate points.

Conical folds could be generated (Fig. S4 in the online version at https://doi.org/10.1016/B978-0-12-814048-2.00023-5) by scaling curves *AB* and *CD* with respect to each other from the upright fold shown in Fig. 4A. This conical fold has been generated by providing the following coordinates:

```
pts = {{{1, 0, 0}, {0.5, 1, 0}, {0, 2, 0}, {0, 3, 0}},{{1, 0, 0.5}, {1, 1, 1},
      {1, 2, 2}, {1, 3, 3}},{{2, 0, 0.5}, {2, 1, 1}, {2, 2, 2}, {2, 3, 3}},{{2, 0, 0},
      {2.5, 1, 0}, {3, 2, 0}, {3, 3, 0}}};
```

It should be noted that the curve *AB* has been scaled down from curve *CD* of the surface *ABCD*. This produced a conical surface from a cylindrical fold.

A plunging fold (Fig. S5B in the online version at https://doi.org/10.1016/B978-0-12-814048-2.00023-5) has been developed from the inclined surface *ABCD* shown in Fig. S5A in the online version at https://doi.org/10.1016/B978-0-12-814048-2.00023-5. Coordinates that have been provided for the surface shown in Fig. S5A in the online version at https://doi.org/10.1016/B978-0-12-814048-2.00023-5 are:

```
pts = {{{0, 0, 0}, {0, 1, 1}, {0, 2, 2}, {0, 3, 3}},
      {{1, 0, 0}, {1, 1, 1}, {1, 2, 2}, {1, 3, 3}},
      {{2, 0, 0}, {2, 1, 1}, {2, 2, 2}, {2, 3, 3}},
      {{3, 0, 0}, {3, 1, 1}, {3, 2, 2}, {3, 3, 3}}};
```

Now by increasing the *z*-values (by adding 3) of the intermediate controlling points, as listed here, the inclined plane could be converted into a plunging fold:

```
pts = {{{0, 0, 0}, {0, 1, 1}, {0, 2, 2}, {0, 3, 3}},
      {{1, 0, 3}, {1, 1, 4}, {1, 2, 5}, {1, 3, 6}},
      {{2, 0, 3}, {2, 1, 4}, {2, 2, 5}, {2, 3, 6}},
      {{3, 0, 0}, {3, 1, 1}, {3, 2, 2}, {3, 3, 3}}};
```

PROBLEM 2: IN THE FRAMEWORK AS PREVIOUSLY STATED, CAN YOU MODIFY THE TIGHTNESS OF THE FOLD?

Answer: Tightness of the fold (gentle, open, close, tight, isoclinal, etc.) can be changed by simply driving sides AD and BC closer or by lifting (by adding *z*-values) the intermediate control points. Fig. S6 in the online version at https://doi.org/10.1016/B978-0-12-814048-2.00023-5 shows five folds with different degrees of tightness, which have been developed by adding coordinates in the intermediate controlling points by adding *z*-values.

By lowering the middle controlling points of the surface *ABCD*, anticlastic antiform (see Lisle and Toimil, 2007) can be prepared (Fig. S7 in the online version at https://doi.org/10.1016/B978-0-12-814048-2.00023-5). For that, two folded sides of the surface have to be at higher elevation then the middle portion. The *z*-values of the middle eight points have been lowered down from two sides to create this shape (coordinates as listed in Appendix 1).

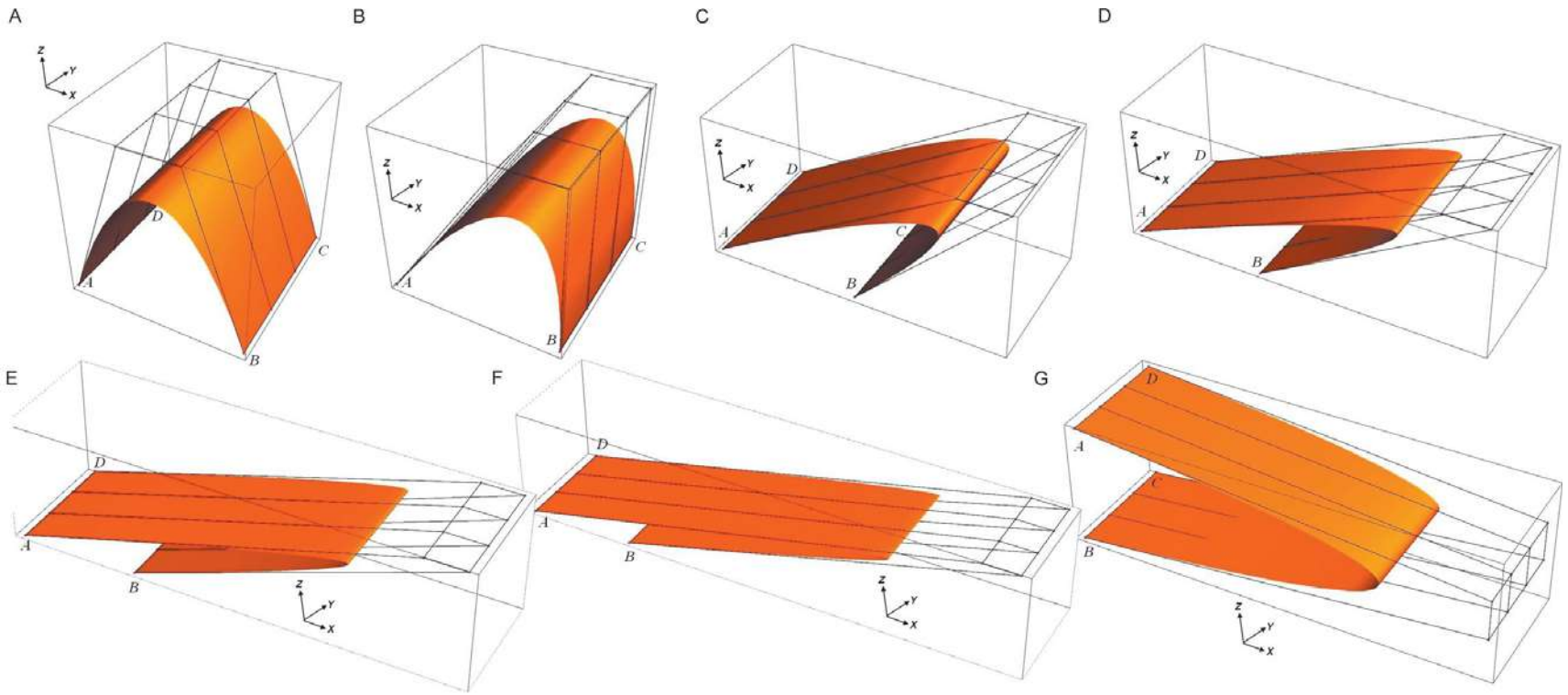

FIG. 4 (A) An upright or symmetric fold, followed by (B–F) asymmetric folds (gently, moderately and steeply inclined), and (G) recumbent fold.

By inverting Fig. 3A, cylindrical synforms (Fig. 5A) and by inverting Fig. 3B, a synclastic synform (Fig. 5C) can be constructed by subtracting the *z*-values of points that already have and by adding *z*-values to other points. Similarly, altering the coordinates of model shown in Fig. S7 in the online version at https://doi.org/10.1016/B978-0-12-814048-2.00023-5, an anticlastic synform (Fig. 5B) could be constructed (coordinates as listed in Appendices 2–4). To invert the surface, points that already possess *z*-values are to be lowered to the points of having no values earlier.

The cubic Bézier surface also has the capability to generate surfaces developed from fold interference. Three examples of superimposed folds viz., Type 0 (Fig. 6), Type 1 (Fig. 7), and Type 2 (Fig. 8) as described by Ramsay (1967) can be produced (Appendices 5–7).

Fig. 9 presents another exercise on a cylindrical fold. Here the fold has been stretched with the help of intermediate central controlling points (Fig. 9B and C), by changing the horizontal positions (*x-axis*) beyond the controlling points of the two limbs of the folded plane. Fig. 9C shows a fan-fold achieved by the following coordinates:

```
pts ={{{0, 0, 0}, {0, 1, 0}, {0, 2, 0}, {0, 3, 0}},
      {{-3, 0, 3}, {-3, 1, 3}, {-3, 2, 3}, {-3, 3, 3}},
      {{6, 0, 3}, {6, 1, 3}, {6, 2, 3}, {6, 3, 3}},
      {{3, 0, 0}, {3, 1, 1}, {3, 2, 2}, {3, 3, 3}}};
```

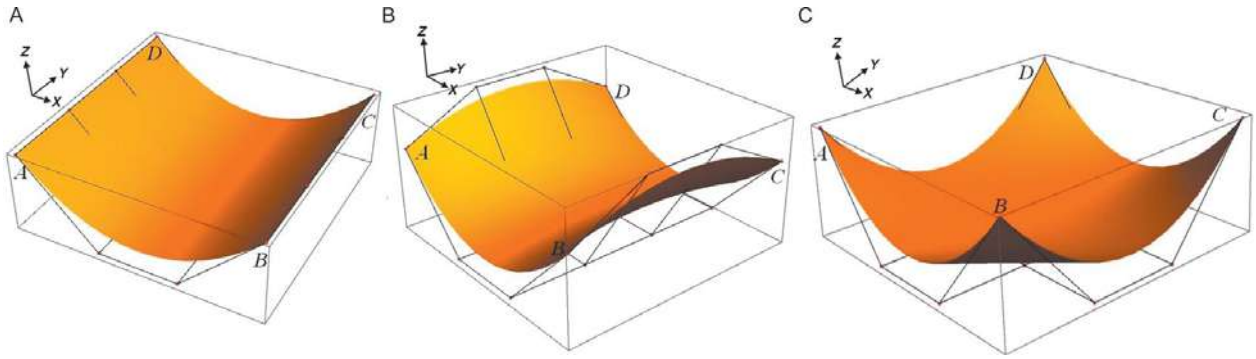

FIG. 5 Examples of (A) cylindrical synforms, (B) anticlastic synform, and (C) synclastic synform.

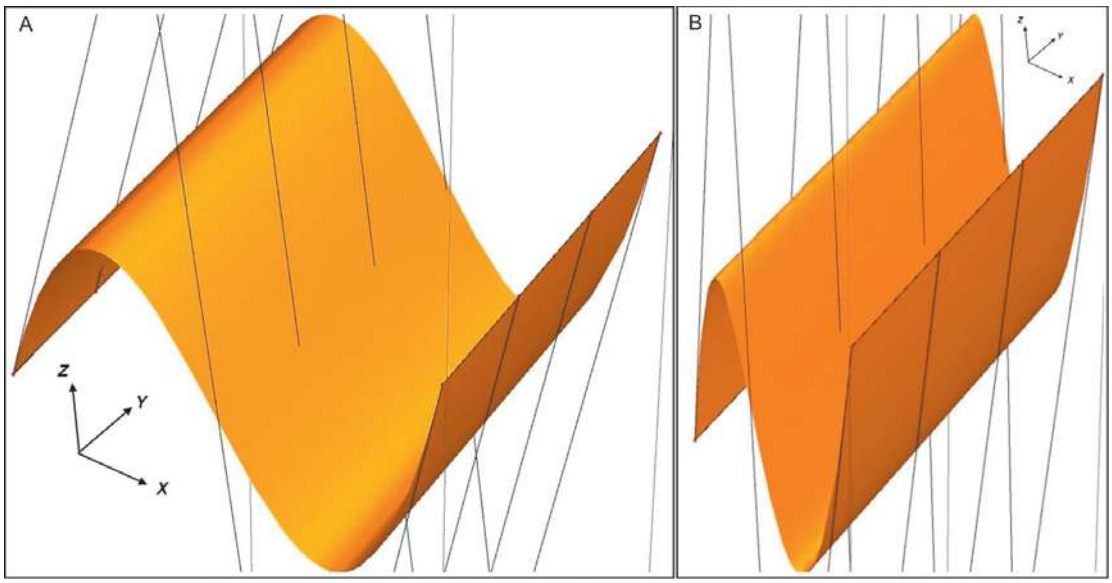

FIG. 6 Construction of Type 0 fold superposition of (A) the first fold with (B) the second fold.

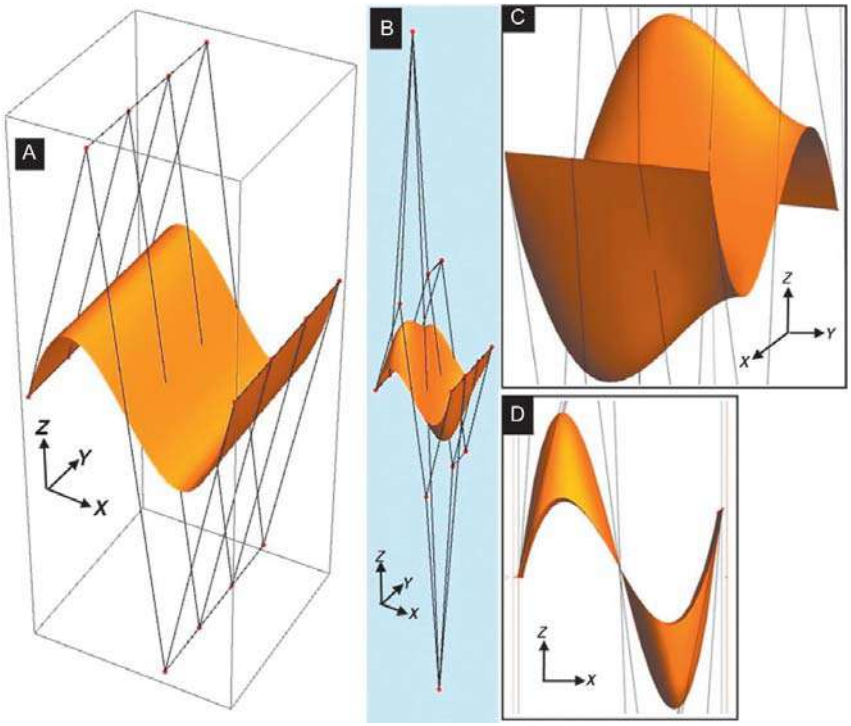

FIG. 7 (B–D) Type 1 folds superposition of (A) the first fold with the second fold.

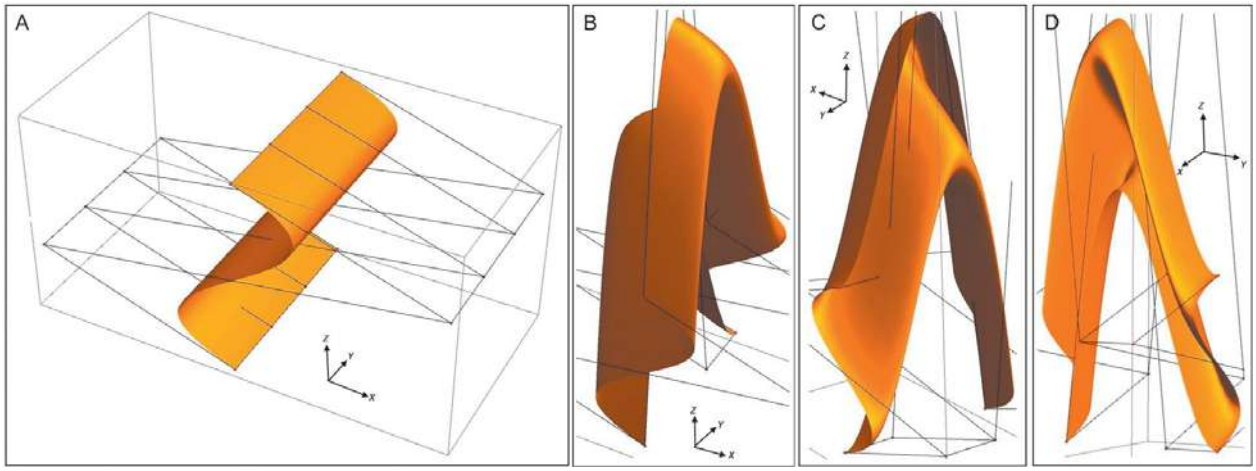

FIG. 8 (B–D) Type 2 folds superposition of (A) the first fold with the second fold.

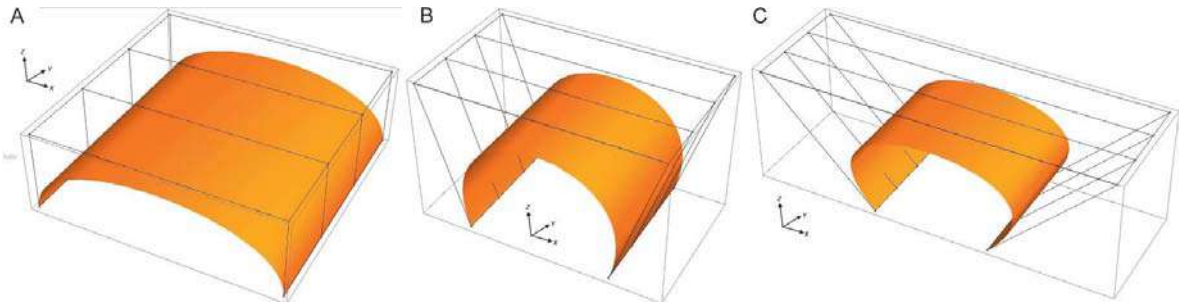

FIG. 9 Box-type-like fold geometry produced in 3D.

3 DISCUSSIONS AND CONCLUSIONS

The Bézier surface has been used in this work to produce single and double generations of folds in 3D. The method is quick, works on simple working principles, and do not have genetic implications at this moment. Previous authors, such as De Paor (1996) and Srivastava and Lisle (2004), fitted Bézier and other curves with folds in 2D. A 3D approach in the same line so far was missing. Because 3D coordinates of any folded morphology is unavailable in a digitized way, the present work cannot be extended readily on natural 3D folds.

The Bézier surface works with a lattice network of controlling points. Here, cubic Bézier surface has been exercised for synthesis of different kinds of folded planes. Cubic Bézier surface provides a grid of 16 controlling points. The corner points define the cylindrical nature of the folds, whereas the intermediate side and central controlling points govern the symmetry and the topography of the folded plane. Horizontal and vertical positions of the central points with respect to the side and corner points defines the characters of the limbs. Wolfram Mathematica provides a platform symbolic programming, which is flexible enough to construct the Bézier surface with symbolic operations and by numeric input of the coordinates of the controlling points. It has enormous opportunities for structural geologist to explore simulation of folds in 3D.

Folded basements have been reported from several places of the world (e.g., Kranck, 1959; Bump, 2003). If the 3D configurations of such folds are deciphered (geophysically), those can be fitted by Bézier surfaces.

Supplementary figures (Figs. S1–S7 in the online version at https://doi.org/10.1016/B978-0-12-814048-2.00023-5), their captions, and some Background information are displayed in: http://www.geos.iitb.ac.in/index.php/en/sm-publications.

Acknowledgments

IIT Bombay provided SM a research sabbatical for the year 2017 and a flexible CPDA research grant. Ake Fagereng and Andrea Billi are thanked for reviewing this chapter. Tasha Frank, Amy Shapiro, and the Elsevier proofreading team are acknowledged for assistance.

APPENDIX 1

For models shown in Fig. S7 in the online version at https://doi.org/10.1016/B978-0-12-814048-2.00023-5.

```
pts. = {{{0, 0, 1}, {0, 1, 0}, {0, 2, 0}, {0, 3, 1}},
        {{1, 0, 3}, {1, 1, 1}, {1, 2, 1}, {1, 3, 3}},
        {{2, 0, 3}, {2, 1, 1}, {2, 2, 1}, {2, 3, 3}},
        {{3, 0, 1}, {3, 1, 0}, {3, 2, 0}, {3, 3, 1}}};
```

APPENDIX 2

For models shown in Fig. 5A

```
pts. = {{{0, 0, 1}, {0, 1, 1}, {0, 2, 1}, {0, 3, 1}},
        {{1, 0, 0}, {1, 1, 0}, {1, 2, 0}, {1, 3, 0}},
        {{2, 0, 0}, {2, 1, 0}, {2, 2, 0}, {2, 3, 0}},
        {{3, 0, 1}, {3, 1, 1}, {3, 2, 1}, {3, 3, 1}}};
```

APPENDIX 3

For models shown in Fig. 5C

```
pts. = {{{0, 0, 2}, {0, 1, 0}, {0, 2, 0}, {0, 3, 2}},
        {{1, 0, 0}, {1, 1, 0}, {1, 2, 0}, {1, 3, 0}},
        {{2, 0, 0}, {2, 1, 0}, {2, 2, 0}, {2, 3, 0}},
        {{3, 0, 2}, {3, 1, 0}, {3, 2, 0}, {3, 3, 2}}};
```

or

```
pts. = {{{0, 0, 2}, {0, 1, 1}, {0, 2, 1}, {0, 3, 2}},
        {{1, 0, 1}, {1, 1, 0}, {1, 2, 0}, {1, 3, 0}},
        {{2, 0, 1}, {2, 1, 0}, {2, 2, 0}, {2, 3, 0}},
        {{3, 0, 2}, {3, 1, 1}, {3, 2, 1}, {3, 3, 2}}};
```

APPENDIX 4

For models shown in Fig. S5B in the online version at https://doi.org/10.1016/B978-0-12-814048-2.00023-5

```
pts. = {{{0, 0, 2}, {0, 1, 3}, {0, 2, 3}, {0, 3, 2}},
        {{1, 0, 0}, {1, 1, 0}, {1, 2, 0}, {1, 3, 0}},
        {{2, 0, 0}, {2, 1, 0}, {2, 2, 0}, {2, 3, 0}},
        {{3, 0, 2}, {3, 1, 3}, {3, 2, 3}, {3, 3, 2}}};
```

or

```
pts. = {{{0, 0, 2}, {0, 1, 3}, {0, 2, 3}, {0, 3, 2}},
        {{1, 0, 0}, {1, 1, 1}, {1, 2, 1}, {1, 3, 0}},
        {{2, 0, 0}, {2, 1, 1}, {2, 2, 1}, {2, 3, 0}},
        {{3, 0, 2}, {3, 1, 3}, {3, 2, 3}, {3, 3, 2}}};
```

APPENDIX 5

For models shown in Fig. 6

```
pts. = {{{0, 0, 0}, {0, 1, 0}, {0, 2, 0}, {0, 3, 0}},
        {{1, 0, 15}, {1, 1, 15}, {1, 2, 15}, {1, 3, 15}},
        {{2, 0, −15}, {2, 1, −15}, {2, 2, −15}, {2, 3, −15}},
        {{3, 0, 0}, {3, 1, 0}, {3, 2, 0}, {3, 3, 0}}};
```

APPENDIX 6

For models shown in Fig. 7

```
pts. = {{{0, 0, 0}, {0, 1, 0}, {0, 2, 0}, {0, 3, 0}},
        {{1, 0, 8}, {1, 1, 29}, {1, 2, 8}, {1, 3, 8}},
        {{2, 0, −8}, {2, 1, −29}, {2, 2, −8}, {2, 3, −8}},
        {{3, 0, 0}, {3, 1, 0}, {3, 2, 0}, {3, 3, 0}}};
```

APPENDIX 7

For models shown in Fig. 8

```
pts. = {{{2, 0, 0}, {2, 1, 0}, {2, 2, 0}, {2, 3, 0}},
        {{−3, 0, 1}, {−3, 1, 1}, {−3, 2, 1}, {−3, 3, 1}},
        {{7, 0, 2}, {7, 1, 2}, {7, 2, 2}, {7, 3, 2}},
        {{2, 0, 3}, {2, 1, 3}, {2, 2, 3}, {2, 3, 3}}};
```

Followed by changes as listed here:

```
pts. = {{{2, 0, 0}, {2, 1, 5}, {2, 2, 5}, {2, 3, 0}},
        {{−3, 0, 1}, {−3, 1, 6}, {−3, 2, 6}, {−3, 3, 1}},
        {{7, 0, 2}, {7, 1, 7}, {7, 2, 7}, {7, 3, 2}},
        {{2, 0, 3}, {2, 1, 8}, {2, 2, 8}, {2, 3, 3}}};
```

References

Agoston, M.K., 2005. Computer Graphics and Geometric Modeling: Implementation and Algorithms. Springer-Verlag, London. p. 907.
Alsop, I., Carreras, J., 2007. The structural evolution of sheath folds: a case study from Cap de Creus. J. Struct. Geol. 29, 1915–1930.
Alsop, I., Carreras, J., 2009. Three dimensional sheath folds in quartz mylonite, Cap de Creus. J. Struct. Geol. 31, 1–2.
Billings, M.P., 1954. Structural Geology. Prentice-Hall, Englewood Cliffs, NJ.

Bump, A.P., 2003. Reactivation, trishear modeling, and folded basement in Laramide uplifts: Implications for the origins of intracontinental faults. GSA Today 13, 4–10.
Clark, R.H., McIntyre, D.B., 1951. A macroscopic method of fabric analysis. Am. J. Sci. 249, 755–768.
Cobbold, P.R., Quinquis, H., 1980. Development of sheath folds in shear regimes. J. Struct. Geol. 1/2, 119–126.
Cornish, S., Searle, M., 2017. 3D geometry and kinematic evolution of the Wadi Mayh sheath fold, Oman, using detailed mapping from high-resolution photography. J. Struct. Geol. 101, 26–42.
De Paor, D., 1996. Bézier curves and geological design. Comput. Meth. Geosci. 15, 389–417.
de Paor, D.G., Dordevic, M.M., Karabinos, P., Tewksbury, B.J., Whitmeyer, S.J., 2016. The fold analysis challenge: a virtual globe-based educational resource. J. Struct. Geol. 85, 85–94.
Donath, F.A., 1964. Strength variation and deformation behavior in anisotropic rocks. In: Judd, W.R. (Ed.), State of Stress in the Earth's Crust. American Elsevier, New York, pp. 281–297.
Farin, G., 1997. Curves and Surfaces for CAGD. Academic Press, p. 429.
Fletcher, R.C., 1991. Three-dimensional folding of an embedded viscous layer in pure shear. J. Struct. Geol. 13, 87–96.
Fleuty, M.J., 1964. The description of folds. Proc. Geol. Assoc. 75, 461–492.
Fossen, H., 2016. Structural Geology, second ed. Cambridge University Press, ISBN: 978-1-107-05764-7. ISBN.
Gogoi, M.P., Mukherjee, S., Goswami, T.K., 2017. Analyses of fold profiles by changing weight parameters of NURB curves. J. Earth Sys. Sci. 126, 98.
Grose, L., Laurent, G., Ailleres, L., Armit, R., Jessel, M., Caumon, G., 2017. Structural data constraints for implicit modeling of folds. J. Struct. Geol. 104, 80–92.
Hall, S.J., 1815. On the vertical position and convolutions of certain strata, and their relation with granite. Trans. R. Soc. Edinb. 7, 79–108.
Hudleston, P.J., 1973. Fold morphology and some implications of theories of fold development. Tectonophysics 16, 1–46.
Janke, S.J., 2015. Mathematical Structures for Computer Graphics. John Wiley & Sons, Inc. ISBN: 978-1-118-71219-1. pp. 223–230.
Kranck, E.H., 1959. On folding-movements in the zone of the basement. Geol. Rundsch. 46, 261–282.
Lemaitre, G.R., 2009. Astronomical Optics and Elasticity Theory: Active Optics Method. Pp. 116, Springer-Verlag, Berlin, ISBN: 978-3-540-68904-1. ISBN.
Lisle, R.J., 1992. Constant bed-length folding: three-dimensional geometrical implications. J. Struct. Geol. 14, 245–252.
Lisle, R.J., Toimil, N.C., 2007. Defining folds on three-dimensional surfaces. Geology 35, 519–522.
Mukherjee, S., Koyi, H.A., Talbot, C., 2012. Implications of channel flow analogue models in extrusion of the higher Himalayan shear zone with special reference to the out-of-sequence thrusting. Int. J. Earth Sci. 101, 253–272.
Mukherjee, S., Punekar, J., Mahadani, T., Mukherjee, R., 2015. A review on intrafolial folds and their morphologies from the detachments of the western Indian Higher Himalaya. In: Mukherjee, S., Mulchrone, K.F. (Eds.), Ductile Shear Zones: From Micro- to Macro-scales. Wiley Blackwell, pp. 182–205.
Mynatt, I., Bergbauer, S., Pollard, D.D., 2007. Using differential geometry to describe 3-D folds. J. Struct. Geol. 29, 1256–1266.
Ramón, M., Pueyo, E.L., Rodríguez-Pintó, A., Ros, L.H., Pocoví, A., Briz, J.L., Ciria, J.C., 2013. A computed tomography approach for understanding 3D deformation patterns in complex folds. Tectonophysics 593, 57–72.
Ramsay, J.G., 1967. Folding and Fracturing of Rocks. McGraw-Hill, New York.
Rowan, M.G., 1997. Three-dimensional geometry and evolution of a segmented detachment fold, Mississippi fan fold belt, Gulf of Mexico. J. Struct. Geol. 19, 463–480.
Sederberg TW (2016) Computer aided geometric design course notes, September 28.
Srivastava, D.C., Lisle, R., 2004. Rapid analysis of fold shape using Bézier curves. J. Strut. Geol. 26, 1553–1559.
Tavani, S., Corradetti, A., Billi, A., 2016. High precision analysis of an embryonic extensional fault-related fold using 3D orthorectified virtual outcrops: the viewpoint importance in structural geology. J. Struct. Geol. 86, 200–210.
Tipper, J.C., 1976. The study of geological objects in three dimensions by the computerized reconstruction of serial sections. J. Geol. 84, 476–484.
Turner, F.J., Weiss, L.E., 1963. Structural Analysis of Metamorphic Tectonites. McGraw-Hill, New York.
Vince, J., 2010. Mathematics for Computer Graphics, third ed. Springer-Verlag, London. p. 310.
von Tscharner, M., Schmalholz, S.M., Epard, J.-L., 2016. 3-D numerical models of viscous flow applied to fold nappes and the Rawil depression in the Helvetic nappe system (western Switzerland). J. Struct. Geol. 82, 32–46.
Wegmann, C.E., 1929. Beispiele tektonischer Analysen des Grundgebirges in Finnland. Bull. Comm. Géol. Finlande 87, 98–127.
Wex, S., Passchier, C.W., de Cemp, E.A., Ilham, S., 2014. 3D visualization of sheath folds in Ancient Roman marble wall coverings from Ephesos. Turkey. J. Struct. Geol. 67, 129–139.
Wilkerson, M.S., Medwedeff, D.A., Marshak, S., 1991. Geometrical modeling of fault-related folds: a pseudo-three-dimensional approach. J. Struct. Geol. 13, 801–812.
Yamamoto, J.K., Koike, K., Kikuda, A.T., da Cruz Campanha, G.A., Endlen, A., 2014. Post-processing for uncertainty reduction in computed 3D geological models. Tectonophysics 214, 232–245.
Zulauf, G., Zulauf, J., Maul, H., 2017. Quantification of the geometrical parameters of non-cylindrical folds. J. Struct. Geol. 100, 120–129.

Further Reading

Steven, J.J., 2015. Mathematical Structures for Computer Graphics. John Wiley & Sons, Inc., ISBN: 978-1-118-71219-1. pp. 223–230.
Wibberley, C.J., 1997. Three-dimensional geometry, strain rates and basement deformation mechanisms of thrust-bend folding. J. Struct. Geol. 19, 535–550.